HHS Public Access
Author manuscript
Traffic. Author manuscript; available in PMC 2023 February 01.

Published in final edited form as:
Traffic. 2022 February ; 23(2): 109–119. doi:10.1111/tra.12828.

Bro1 binds the Vps20 subunit of ESCRT-III and promotes ESCRT-III regulation by Doa4

Dalton Buysse[1], **Matt West**[1], **Mitchell Leih**[1], **Greg Odorizzi**[1,2]

[1]Department of Molecular Cellular and Developmental Biology, University of Colorado, Boulder, CO 80309, USA

Abstract

The budding of intralumenal vesicles (ILVs) at endosomes requires membrane scission by the ESCRT-III complex. This step is negatively regulated in yeast by Doa4, the ubiquitin hydrolase that deubiquitinates transmembrane proteins sorted as cargoes into ILVs. Doa4 acts non-enzymatically to inhibit ESCRT-III membrane scission activity by directly binding the Snf7 subunit of ESCRT-III. This interaction inhibits the remodeling/disassembly of Snf7 polymers required for the ILV membrane scission reaction. Thus, Doa4 is thought to have a structural role that delays ILV budding while it also functions enzymatically to deubiquitinate ILV cargoes. In this study, we show that Doa4 binding to Snf7 in vivo is antagonized by another ESCRT-III subunit, Vps20. Doa4 is restricted from interacting with Snf7 in yeast expressing a mutant Vps20 allele that constitutively binds Doa4. This inhibitory effect of Vps20 is suppressed by overexpression of another ESCRT-III-associated protein, Bro1. We show that Bro1 binds directly to Vps20, suggesting that Bro1 has a central role in relieving the antagonistic relationship that Vps20 has toward Doa4.

Graphical Abstract

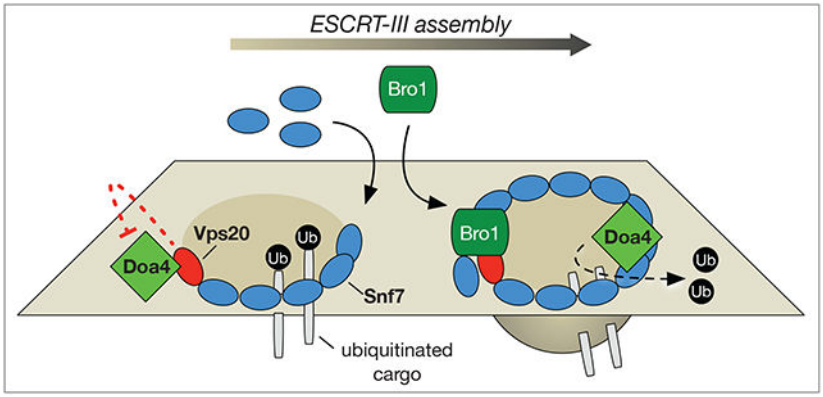

[2]Author for correspondence (odorizzi@colorado.edu).

AUTHOR CONTRIBUTIONS

Conceptualization: D.B., G.O.; Methodology: D.B., G.O.; Formal analysis: D.B., G.O., M.W.; Investigation: D.B., M.W.; Resources: D.B., G.O.; Writing - original draft: D.B.; Writing - review & editing: D.B., G.O.; Visualization: D.B., M.W.; Supervision: G.O.; Project administration: G.O.; Funding acquisition: G.O.

COMPETING INTERESTS

The authors declare no competing interests.

In yeast, the Doa4 ubiquitin hydrolase deubiquitinates transmembrane proteins sorted as cargoes into intralumenal vesicles at endosomes. Doa4 also functions non-catalytically by binding the Snf7 subunit of the ESCRT-III complex, which regulates the membrane scission activity of ESCRT-III. The calaytic and non-catalytic functions of Doa4 are inhibited through its interaction with the Vps20 subunit of ESCRT-III. This inhibition is relieved by the Bro1 protein, which binds directly to Vps20.

Keywords

Yeast; Endosome; Membrane Scission; Ubiquitin Hydrolase

INTRODUCTION

The Endosomal Sorting Complexes Required for Transport (ESCRTs) comprise a broadly conserved machinery that functions at many different cellular locations (reviewed in Schöneberg et al., 2016). At endosomes, ESCRT complexes 0, I, and II function to sort ubiquitinated transmembrane proteins as cargoes into intralumenal vesicles (ILVs). Cargoes are trapped at the site of ILV budding by ESCRT-III (Teis et al., 2010), the subunits of which polymerize in a spiral pattern at the cytosolic surface of the endosomal membrane (Hanson et al., 2008). ESCRT-III assembly also constricts and severs the necks of membrane invaginations, thereby completing the ILV budding process (Wollert et al., 2009).

Prior to their enclosure within ILVs, cargoes must be deubiquitinated in order to replenish the cellular supply of unconjugated ubiquitin (Swaminathan et al., 1999). ILV cargoes are deubiquitinated by ubiquitin hydrolases that are recruited by ESCRT-III (Luhtala and Odorizzi, 2004; Row et al., 2007). In *Saccharomyces cerevisiae*, Doa4 is the ubiquitin hydrolase that deubiquitinates ILV cargoes (Dupré and Haguenauer-Tsapis, 2001; Katzmann et al., 2001; Losko et al., 2001). Doa4 also functions non-enzymatically to regulate ESCRT-III membrane scission activity, suggesting that ILV budding is coordinated with cargo deubiquitination. The non-catalytic N-terminal region of Doa4 directly binds Snf7 (Buysse et al., 2020), which is an ESCRT-III subunit that homopolymerizes to form spiral assemblies (Hanson et al., 2008). In vivo and in vitro, Doa4-binding blocks Snf7 polymer association with the Vps2 and Vps24 subunits of ESCRT-III (Buysse et al., 2020). Vps2 and Vps24 work in tandem to recruit and activate Vps4, which is an AAA-type ATPase that remodels Snf7 polymers by catalyzing subunit turnover (Yang et al., 2015; Mierzwa et al., 2017). This remodeling/disassembly process is essential for ESCRT-III membrane scission activity (Nickerson et al., 2010; Adell et al., 2014). Accordingly, ILV membrane scission is inhibited in vivo by overexpression of either the wild-type *DOA4* gene or the catalytically inactive $doa4^{C571S}$ allele (Johnson et al., 2017). By shielding Snf7 polymers from Vps2 and Vps24, Doa4 appears to delay ILV budding while it deubiquitinates ILV cargoes.

Snf7 homopolymerization is nucleated by the Vps20 subunit of ESCRT-III (Teis et al., 2008; Saksena et al., 2009). Vps20 also binds directly to Doa4 (Richter et al., 2013), and this interaction inhibits both ILV cargo deubiquitination and the regulation of Snf7 polymer remodeling/disassembly by Doa4 (Johnson et al., 2017). Thus, Doa4 is functionally

restricted by Vps20, but it is unclear how this restriction is relieved. In this study, we report interactions that occur in vivo and in vitro between Vps20, Doa4, and Bro1, the latter of which is a cofactor previously shown to stimulate Doa4 ubiquitin hydrolase activity (Richter et al, 2007). From these data, we infer a model in which Bro1 binding to Vps20 mediates the the transition of Doa4 away from its inhibitory interaction with Vps20 so that Doa4 can associate with Snf7.

RESULTS AND DISCUSSION

Vps20 antagonizes Doa4 interaction with Snf7 at yeast endosomes

Yeast Vps20 has a closed/inactive conformation that transitions to an open/active state, the latter of which nucleates Snf7 homopolymerization to launch ESCRT-III assembly (Figure 1A; Saksena et al., 2009). Using intragenic mutations that stabilize each conformational state of Vps20 (Teis et al., 2010), we had previously shown that Doa4 binds the open/active conformation of Vps20 but not the closed/inactive state. Specifically, the N terminal region of Doa4 (amino acids 1–80) directly binds the open/active form of Vps20, which is stabilized by deletion of the amino-acid loop connecting Vps20 helix α1 to helix α2 ($Vps20^{\Delta loop}$; Figure 1A). The segment of Doa4 that binds Vps20 is structurally predicted to comprise a Microtubule Interacting and Trafficking (MIT) domain (Richter et al., 2013; Johnson et al., 2017). The N-terminal region of Doa4 also directly binds the Snf7 subunit of ESCRT-III, although the minimal fragment of Doa4 that has been identified thus far to be required for interaction with Snf7 consists of amino acids 1–348 in Doa4, which overlaps both the MIT-like domain that binds Vps20 and a Rhodanese Homology Domain of unknown function (Buysse et al., 2020; Figure 1A).

The stabilization of Snf7 polymers by Doa4 is inhibited in yeast expressing the open/active mutant $Vps20^{\Delta loop}$ protein, which constitutively binds Doa4 (Johnson et al., 2017). Therefore, we tested the extent to which $Vps20^{\Delta loop}$ expression affected Doa4 interaction with Snf7 in vivo using bimolecular fluorescence complementation (BiFC) microscopy. The coding sequences of the N- or C- terminal fragments of Venus fluorescent protein (VN or VC, respectively) were integrated in frame with the genomic coding sequences of the *DOA4* and *SNF7* genes, resulting in C-terminal fusion proteins (Doa4-VN and Snf7-VC) that were expressed under control of their endogenous promoters. Binding between Doa4 and Snf7 brings VN and VC into close proximity (≤ 7nm), allowing the Venus reporter to fold into its native structure and emit fluorescence (Kerppola, 2006). Although C-terminal VN- or VC-tagging of Snf7 (and other ESCRT-III subunits) disrupts functionality in ILV cargo sorting, it does not impair endosomal localization, making BiFC useful for testing ESCRT-III subunit interactions in vivo (Buysse et al., 2020).

As shown previously (Buysse et al., 2020), BiFC fluorescence that was derived from the interaction between Doa4-VN and Snf7-VC was observed in wild-type cells at endosomal puncta stained with FM 4–64 (Figure 1B), which is a fluorescent lipophilic dye delivered by endocytosis to endosomal and vacuolar membranes (Vida and Emr, 1995). This BiFC fluorescence was reduced by ~75% in $vps20^{\Delta loop}$ cells but was recovered by ~50% upon point-mutation of the Doa4-binding MIM1 sequence in helix α6 of the $Vps20^{\Delta loop}$ protein ($vps20^{\Delta loop\Delta MIM1}$; Figure 1, B and C). Thus, the interaction between Doa4 and Snf7 at

yeast endosomes is antagonized by Vps20 binding via its MIM1 site to Doa4. As expected, deletion of the *VPS20* gene (*vps20Δ*) completely eliminated BiFC fluorescence derived from Doa4-VN interaction with Snf7-VC (Figure 1, B and C) because Snf7 localization to endosomes depends on Vps20 (Teis et al., 2010).

Vps20 might inhibit Doa4 from interacting with Snf7 in vivo if Doa4 binding to Vps20 and Snf7 is mutually exclusive. However, testing this hypothesis has been problematic because neither Vps20 nor the constitutively open/active $Vps20^{\Delta loop}$ protein can bind in vitro to the purified $Doa4^{1–348}$ fragment, even though this region of Doa4 harbors the MIT-like domain (amino acids 1–80) that directly binds Vps20 and $Vps20^{\Delta loop}$ (Richter et al., 2013). We had previously observed that Vps20 binding to the purified Doa4 MIT-like domain is eliminated when the Doa4 fragment is lengthened beyond Ala^{80} (Richter et al., 2013), which suggests that the in-vitro binding activity of the Doa4 MIT domain is sensitive to the structure conferred by amino acids flanking it.

Doa4 interaction with Snf7 in vivo is promoted by Bro1

Using BiFC to characterize the interaction in vivo between Doa4 and Vps20, we had previously shown this interaction is decreased by overexpression of the *BRO1* gene from a high-copy (2μ) plasmid (Johnson et al., 2017; Figure S1). This result, together with the data showing that Vps20-binding inhibits Doa4 interaction with Snf7 (Figure 1), suggested that Bro1 disrupts Vps20 interaction with Doa4 in vivo in order to facilitate Doa4 binding to Snf7. Consistent with this hypothesis, we found that *BRO1* overexpression in wild-type cells resulted in a 50% increase above the basal amount of BiFC fluorescence derived from Doa4-VN interaction with Snf7-VC (Figure 2, A–B). Likewise, the inhibition of this BiFC interaction observed in $vps20^{\Delta loop}$ cells was rescued by ~50% upon overexpression of *BRO1* (Figure 2, C–D). These results are consistent with a model in which Bro1 facilitates the transition of Doa4 away from its inhibitory interaction with Vps20 so that Doa4 can associate with Snf7.

Bro1 is comprised of an N-terminal Bro1 Domain (BOD), a central V domain, and a C-terminal proline-rich region (Figure 2E). We had previously shown by BiFC that Bro1 Domain overexpression (2μ *BOD*) disrupts Vps20 binding to Doa4 (Johnson et al., 2017; Figure S1). The same 2μ *BOD* construct, however, failed to enhance Doa4-VN interaction with Snf7-VC, unlike the effect seen with full-length *BRO1* overexpression (Figure 2A–B); likewise, the 2μ *BOD* construct did not phenocopy the effect that full-length *BRO1* overexpression has toward rescuing Doa4-VN interaction with Snf7-VC in $vps20^{\Delta loop}$ cells (Figure 2, C–D). It is noteworthy that the MIM1 sequence in Snf7 helix α6 serves as the binding site for both Doa4 and the Bro1 domain (Wemmer et al., 2011; Buysse et al., 2020); the Bro1 Domain (when overexpressed) might, therefore, out-compete Doa4-VN to interact with Snf7-VC. Alternatively, the 2μ *BOD* construct might not achieve the same level of expression as 2μ *BRO1*, or the Bro1 V domain and proline-rich region (V-Pro) might be necessary for Bro1 to enhance Doa4 interaction with Snf7, though overexpression of the V-Pro region alone (2μ *V-Pro*) did not affect the BiFC interaction between Doa4-VN and Snf7-VC (Figure 2, C–D).

BRO1 overexpression rescues ILV budding and cargo sorting in *vps20$^{\Delta loop}$* cells

We had previously shown by electron tomography that wild-type yeast cells have spherical endosomal multivesicular bodies (MVBs) that contain numerous ILVs (e.g., Nickerson et al., 2006; Figure 3A). We had also reported that *vps20$^{\Delta loop}$* cells have fewer ILVs and fewer spherical MVBs; instead, this mutant strain predominantly contains class E compartments, which are aberrant stacks of flattened endosomal "cisternae" (Johnson et al., 2017; Figure 3B). ILVs account for ~50% of the total membrane content of MVBs in wild-type yeast but only ~7% of the membrane content at class E compartments in *vps20$^{\Delta loop}$* cells (Figure 3D), signifying the inhibitory effect caused by constitutively open/active Vps20. Tomographic modeling showed that the fraction of ILV membrane content in *vps20$^{\Delta loop}$* cells was increased by >50% upon *BRO1* overexpression (Figure 3C–D; Figure S3), which is similar to the recovery in ILV budding that we had previously shown to occur in response to point-mutation of the Doa4-binding MIM1 sequence in the mutant *vps20$^{\Delta loop}$* allele (Johnson et al., 2017). These results were corroborated by a survey of 80-nm thin sections of yeast in which we scored the general morphology of endosomal structures in >100 cell sections. This analysis showed that ~6% of endosomes observed in *vps20$^{\Delta loop}$* cells were MVBs, with the remainder of endosomes in this strain being class E compartments. In contrast, the frequency of MVBs observed in *vps20$^{\Delta loop}$* cells overexpressing *BRO1* was >30% (Figure 3E), mirroring the quantitative recovery of ILV budding that was observed by tomography (Figure 3D).

Using a combination of optical and enzymatic reporter assays, we also found that *BRO1* overexpression rescued ILV cargo sorting in *vps20$^{\Delta loop}$* cells. Cps1 is a transmembrane protein that is transported from the Golgi to endosomes, where the ESCRT machinery sorts Cps1 into ILVs that are delivered into the vacuole lumen upon endosome – vacuole fusion. Failure to sort Cps1 into ILVs results in the delivery of this cargo to the vacuole membrane (Odorizzi et al., 1998). We observed by confocal fluorescence microscopy that *BRO1* overexpression rescued the sorting of GFP-Cps1 into the vacuole lumen of *vps20$^{\Delta loop}$* cells, though we occasionally saw cells in this population with GFP-Cps1 at the vacuole membrane (Figure 3F). Using a quantitative enzymatic assay that measures the sorting of firefly luciferase fused to Cps1 (Nickerson and Merz, 2015), we determined that *BRO1* overexpression rescued Cps1 sorting by ~40% (Figure 3G). These results were also observed using similar optical and enzymatic analyses of another ILV cargo protein, Sna3 (Figure S2).

The observations described above explain our earlier study showing that ILV budding is defective in *bro1Δ* cells but rescued in this strain upon mutation of the MIM1 sequence in Vps20 that binds Doa4; notably, this recovery in ILV budding requires Doa4 expression but not the ubiquitin hydrolase activity of Doa4 (Richter et al., 2013). Collectively, these data point to Bro1 functioning to relieve Doa4 from inhibition by Vps20 so that Doa4 can function non-enzymatically to promote ILV budding. The results in Figure 2 showing that Bro1 facilitates Doa4 interaction with Snf7 in vivo suggest that Doa4 binding to Snf7 is the means by which Doa4 positively influences ILV budding even though the final step in this process, ILV membrane scission, requires the remodeling/disassembly of Snf7 polymers, which Doa4 inhibits through its interaction with Snf7 (Buysse et al., 2020). This contradictory relationship might be explained by measurements showing that in wild-type

yeast, the abundance of Doa4 is 30–50% that of Snf7 (Ho et al., 2018). Conceivably, the ILV budding process could proceed more efficiently when Snf7 polymer remodeling/disassembly is negatively regulated by the more limited quantities of Doa4 that exist under normal physiological conditions. Doa4 is not strictly essential for ILV budding because MVBs/ILVs are observed in cells lacking Doa4 expression (Richter et al., 2007); in this circumstance, however, cellular levels of free non-conjugated ubiquitin are depleted (Swaminathan et al., 1999), which greatly reduces the abundance of ubiquitinated cargoes. Based on the observation that ubiquitinated cargoes stimulate ILV formation (MacDonald et al., 2012), the fewer number of cargoes in cells lacking Doa4 could fall below a threshold at which the regulatory function of Doa4 might be needed.

Bro1 directly binds Vps20

The results described above suggest that Bro1 facilitates the transition of Doa4 away from its inhibitory interaction with Vps20 so that Doa4 can associate with Snf7. Given that Bro1 binds directly both to Snf7 and to Doa4 (Kim et al., 2005; Richter et al., 2007), we considered the possibility that Bro1, when bound to Snf7, recruits Doa4 away from Vps20. However, this model cannot explain why Doa4 interaction with Vps20 in vivo is inhibited by Bro1 Domain overexpression because, although the Bro1 Domain binds Snf7 (Kim et al., 2005), it lacks the Doa4-binding site (Richter et al., 2007).

An alternative model to explain how Bro1 facilitates Doa4 transition away from Vps20 to Snf7 is through direct binding of Vps20 by the Bro1 Domain. We first tested this model using BiFC to determine if Vps20 interacts with the Bro1 Domain in vivo. Indeed, we observed BiFC fluorescence in cells co-expressing Vps20-VC and Bro1 Domain-VN. This BiFC fluorescence was eliminated upon deletion of Vps25 (*vps25Δ*; Figure 4A–B), which is a subunit of the ESCRT-II complex required for Vps20 localization (Teis et al., 2010). However, deletion of Doa4 (*doa4Δ*) did not affect the BiFC fluorescence derived from interaction between Vps20-VC and Bro1 Domain-VN (Figure 4A–B), signifying that Vps20 interacts in vivo with the Bro1 Domain independently of Vps20 binding to Doa4.

We next co-expressed GST-Bro1 Domain together with wild-type or mutant Vps20 proteins in *E. coli* to test for their interaction with one another in a heterologous system lacking other yeast proteins. Following their affinity isolation from bacterial lysates using glutathione-sepharose, proteins were resolved by SDS-PAGE and examined by western blotting with antibodies against GST versus Vps20 (Johnson et al., 2017). As shown in Figure 4C, GST-Bro1 Domain bound the constitutively open/active $Vps20^{\Delta loop}$ protein but did not bind wild-type Vps20, suggesting the latter protein predominantly adopts the closed/inactive conformation when expressed alone in bacteria. Consistent with this interpretation, GST-Bro1 Domain also did not bind the mutant $Vps20^{PW}$ protein, which has intragenic mutations that stabilize Vps20 in the closed/inactive state (Teis et al., 2010). Thus, as in the case of Doa4, Bro1 directly binds the open/active conformation of Vps20. The Bro1 Domain fused to a C-terminal HA tag similarly bound the $Vps20^{\Delta loop}$ protein when co-expressed in bacteria and affinity purified using anti-HA antibodies linked to agarose beads (Figure S4A). We also co-expressed in bacteria Bro1 Domain-HA and $Vps20^{\Delta loop}$ with GST fused to $Doa4^{2–80}$, the N-terminal region of Doa4 that directly binds $Vps20^{\Delta loop}$ (Richter et al.,

2013). Glutathione-sepharose pulldown of GST-Doa4$^{2–80}$ from bacterial lysates resulted in the co-isolation of Vps20$^{\Delta loop}$ but not Bro1 Domain-HA (Figure S4B), consistent with a model in which Vps20 does not bind simultaneously to both Doa4 and Bro1.

We tested the nature by which the Bro1 Domain directly binds Vps20$^{\Delta loop}$ by mutating either the MIM1 sequence in Vps20 helix α6 or the MIM2 sequence located in the linker region between Vps20 helix α5 and helix α6. As noted above, the MIM1 sequence is required for direct binding of Vps20$^{\Delta loop}$ to the MIT domain of Doa4 (Richter et al., 2013), but point-mutation of this site did not disable Vps20$^{\Delta loop}$ binding to GST-Bro1 Domain (Figure 4C). Likewise, binding of GST-Bro1 Domain still occurred upon point mutation of the Vps20 MIM2 sequence (Figure 4C), which is the site through which Vps20 interacts with the MIT domain of Vps4 (Kieffer et al., 2008). We also tested if mutation of Patch 1 in the Bro1 Domain disrupts its interaction with Vps20$^{\Delta loop}$. Patch 1 is the site in the Bro1 Domain that mediates a direct interaction with the MIM1 sequence in Snf7 (Kim et al., 2005; McCullough et al., 2008), but point mutation of Patch 1 in the Bro1 Domain (ΔP1) did not affect its binding to the Vps20$^{\Delta loop}$ protein (Figure 4C). Thus, the Bro1 Domain binds Vps20 differently from the MIM-based binding mechanisms that Vps20 and Snf7 employ.

We also found that GST-Bro1 Domain binding to Vps20$^{\Delta loop}$ was unaffected by point-mutation of Patch 2 in the Bro1 Domain (ΔP2; Figure 4C). This highly conserved sequence has a tyrosine residue that is phosphorylated by Src kinase in *Xenopus* and human orthologs of Bro1 (Che et al., 1995; Schmidt et al., 2005). Tyrosine phosphorylation is rare in *S. cerevisiae*, and mutation of Patch 2 in yeast Bro1 has no observable impact in ILV cargo sorting (Kim et al., 2005); thus, the function of this highly conserved site in Bro1 is unknown. The only mutation we tested that disabled the interaction between GST-Bro1 Domain and Vps20$^{\Delta loop}$ was deletion of C-terminal amino acids 171–221 in Vps20 (ΔloopΔC; Figure 4C). The ΔC truncation eliminates Vps20 helix α5-linker-α6, suggesting that this region of Vps20 harbors the binding site for the Bro1 Domain.

We have shown that Doa4 binding to Snf7 in vivo is antagonized by another ESCRT-III subunit, Vps20, and that this inhibitory effect is suppressed by Bro1. Our finding that Bro1, like Doa4, binds directly to Vps20 suggests that Bro1 has a central role in relieving the antagonistic relationship that Vps20 has toward Doa4 (Figure 5). Because Bro1 and Doa4 both bind directly to Vps20 and to Snf7 (Kim et al., 2005; Richter et al., 2013; Buysse et al., 2020; this study), the timing of these interactions are likely to be coordinated. Competition between Doa4 and Bro1 might regulate their interactions with Vps20 and/or Snf7, which would explain the effects of Bro1 overexpression that were observed in this study. This coordination might also be influenced by binding of the Bro1 Domain to ubiquitin (Pashkova et al., 2013), which could serve to increase the local concentration of Bro1 through interactions with ubiquitinated transmembrane cargo proteins that are concentrated by ESCRT complexes 0, I, and II. Because Doa4-mediated deubiquitination of these cargoes prior to their enclosure within ILVs is essential for cells to maintain normal levels of unconjugated ubiquitin (Swaminathan et al., 1999), determining the timing of Bro1 and Doa4 interactions with ESCRT-III will be an important step in understanding the broader coordination that is needed between ESCRT-III membrane scission activity and ubiquitin homeostasis.

MATERIALS AND METHODS

Construction of yeast strains and DNA plasmids

Standard techniques were used for the growth and genetic manipulation of *S. cerevisiae* strains (Table 1) and for the construction of plasmids (Table 2). Yeast strains created for this study were constructed by one-step PCR-based integration using cassettes described in Longtine et al. (1998) and Webster et al. (2014). Plasmids to express mutant derivatives of Bro1 were created by ligating PCR products containing the Bro1$^{I144D;L336D}$ and Bro1$^{PSVF\text{-}AAAA}$ sequences into SpeI/SalI-digested pRS413, resulting in pDCB101 and pDCB102, respectively. A 2μ overexpression vector for *DOA4* was created by ligating the ~3.6 kb XhoI/NotI fragment from pCR30 (Richter et al., 2007) into similarly digested pRS202, resulting in pDCB103. pDCB104 was generated by ligating the XhoI/HindIII fragment from pCR15 (Richter et al., 2007) into pRS202 digested with the same enzymes. To create plasmids expressing mutant derivatives of Vps20, a low-copy-number (*CEN*) vector expressing *VPS20* from its endogenous promoter (pEE2; Babst et al., 2002) was subjected to site-directed mutagenesis to create the Δloop(Δ48–59) and Δloop;ΔMIM1(Δ48–59; P216D;L217D) mutations, resulting in pDCB61 and pDCB63, respectively. The Sna3-LUCID vector was generated by inserting a PCR product containing Sna3-FLuc and PGK1$_p$::RLuc from pDN252 (Nickerson et al., 2012) into linearized pRS415 via homologous recombination in yeast. Plasmids pGO840, pGO843, and pGO844 were generated by ligating a PCR product from pGST-Bro1 Domain (Kim et al., 2005) into BspEI/MluI-digested pGO511, pGO816, and pGO817 (Johnson et al., 2017), respectively. Plasmids pDCB21 and pDCB35 were generated via site-directed mutagenesis of pGO844 to create the ΔMIM1 and ΔMIM2 mutations in Vps20, respectively. Site-directed mutagenesis was performed on pGST-Bro1 Domain to generate the Δpatch1 and Δpatch2 mutations, and PCR products containing these sequences were ligated into BspEI/MluI-digested pGO844 to create pDCB45 and pDCB47, respectively. Plasmid pDCB51 was generated by ligating a PCR product containing the Vps20$^{1–170;\Delta 48–59}$ sequence into SacI/KpnI-digested pGO840. Plasmids pGO896 and pGO897 were generated by ligating into the SmaI site of pGO817 and pGO826 (respectively) a PCR product containing a Shine-Dalgarno sequence followed by the Bro1$^{1–387}$ coding sequence followed in frame by one copy of the HA epitope coding sequence then followed by a stop codon.

Pulldown of recombinant proteins from bacteria

For pulldown of Vps20 or mutant derivatives with GST-Bro1$^{1–387}$, HA-Bro1$^{1–387}$, or GST-Doa4$^{2–80}$ fusion proteins, 10-mL liquid cultures of *E. coli* strain C41 (DE3) cells transformed with recombinant plasmids to co-express proteins were induced with 0.5 mM isopropyl β-D-1-thiogalactopyranoside at 20°C for 16 hours. Cultures were then centrifuged at 1800 × g for 10 min to harvest the bacterial cells, then lysed in phosphate-buffered saline (PBS) containing 1 mg/mL lysozyme (Roche), 0.25U of Benzonase nuclease (Sigma-Aldrich) and 1mM phenylmethylsulfonyl fluoride (Sigma-Aldrich). Lysates were sonicated at 15W for 15 seconds, then triton X-100 (0.2%) was added, and the lysates were rotated at 4°C for 15 min before clarifying by centrifugation at 16,000 × g for 10 min at 4°C. The resulting supernatants were incubated by inversion with glutathione sepharose beads (GE Healthcare) or anti-HA antibody-linked agarose (Pierce) for 4 hours at 4°C. After 4

washes with PBS + 0.2% TX-100, the beads were dried and boiled in Laemmli buffer. Protein samples were resolved by SDS-PAGE, transferred to a nitrocellulose membrane, and Western blotting was performed using anti-GST monoclonal antibodies (ThermoFisher, catalog #A-5800, 1:10,000), anti-HA monoclonal antibodies (anti-HA) or rabbit polyclonal antisera raised against Snf7 (Babst et al., 1998, 1:10,000) or Vps20 (Johnson et al., 2017, 1:1,000). Detection of these proteins was performed using HRP-conjugated goat-anti-mouse or goat-anti-rabbit secondary antibodies (Sigma-Aldrich catalog #A4416 or A8919, 1:3,000), followed by analysis with the ChemiDoc MP imaging system (Bio-Rad).

Fluorescence microscopy and quantification

Liquid cultures of yeast strains were grown at 30°C to logarithmic phase before staining endosomal membranes with 1.6μM FM4–64 (Invitrogen) for 25 min followed by a 90-min chase in stain-free medium (Odorizzi et al., 2003; Vida & Emr, 1995). Live yeast cells were then observed at room temperature with an inverted fluorescence microscope (Ti2 2E PSF; Nikon) equipped with a Yokogawa CSU-X1 spinning disk confocal system and a 100x (1.45 numerical aperture) oil objective (Plan Apo λ; Nikon). Images taken with an Andor iXON Ultra 512×512 EMCCD camera were acquired with Micromanager version 2.0 software and analyzed with ImageJ software (NIH). Quantification of BiFC images was performed by combining the mean and standard deviation of the fluorescence intensity per cell in at least 50 individual cells per condition. Each condition was repeated on separate days for at least three experimental replicates, and the standard error of the mean was calculated. Statistical significance was calculated in GraphPad Prism software using a non-paired Students *t*-test

Quantitative MVB cargo sorting analysis

Quantitative analysis of Cps1 sorting by LUCID was performed using the dual luciferase assay system (Promega). Cells transformed with pDN278 were harvested at early-logarithmic phase (0.3–0.4 OD_{600}). 1.2 OD_{600} units were then lysed by vortex agitation for 15 min with glass beads in 200 μL of the provided lysis buffer. *Firefly* and *Renilla* luciferase were analyzed in black 96-well plates using a SpectroMax M5 microplate reader (Molecular Devices). Signal from FLuc-Cps1 was normalized to the cytosolic RLuc signal to provide an internal control for plasmid expression. Three readings were performed for each strain per day on four separate days. S.E.M. was plotted and statistical significance was calculated in GraphPad Prism software using a non-paired Student's *t*-test.

Electron microscopy

Liquid cultures of yeast cells were harvested at mid-logarithmic phase, vacuum-filtered on 0.45-μm millipore paper, loaded into 0.5-mm aluminum hats, and high pressure frozen with a Wohlwend HPF (Wohlwend, Switzerland). Cells were freeze-substituted in an Automated Freeze-Substitution machine, (Leica Vienna, Austria) at −90°C in a preparation of 0.1% uranyl acetate and 0.25% gluteraldehyde in anhydrous acetone (Giddings, 2003). Samples were then washed in pure acetone, embedded in Lowicryl HM20 resin (Polysciences), polymerized at −60°C and warmed slowly over 4 days. A Leica UC6 Ultra-Microtome was used to cut 80-nm thick sections, which were placed on Rhodium-plated copper slot grids (Electron Microscopy Sciences). Sections were then stained in 2% uranyl acetate for 10 min and in Reynold's lead citrate for 20 min before imaging with a FEI Tecani T12 Spirit

electron microscope equipped with a 120 kV LaB6 filament and AMT (2k × 2k) CCD. MVBs were identified as spherical structures surrounded by a bilayer and containing at least two ILVs within the lumen. Class E compartments were identified as two or more cisternae (without fenestration) that were at least twice as long as wide. 100 cell profiles were surveyed for each condition. Images were processed with ImageJ software (NIH).

Supplementary Material

Refer to Web version on PubMed Central for supplementary material.

ACKNOWLEDGEMENTS

The authors are very grateful to Larry Gold for generously providing support and to Lee Niswander for critical coordination.

FUNDING

This work was supported by a grant from the National Institutes of Health/National Institute of General Medical Sciences to G.O. (grant number: GM111335).

REFERENCES

Adell MAY, Vogel GF, Pakdel M, Müller M, Lindner H, Hess MW and Teis D (2014). Coordinated binding of Vps4 to ESCRT-III drives membrane neck constriction during MVB vesicle formation. Journal of Cell Biology 205, 33–49.

Babst M, Wendland B, Estepa EJ and Emr SD (1998). The Vps4p AAA ATPase regulates membrane association of a Vps protein complex required for normal endosome function. The EMBO Journal 17, 2982–2993. [PubMed: 9606181]

Babst M, Katzmann DJ, Estepa-Sabal EJ, Meerloo T and Emr SD (2002). Escrt-III: An endosome-associated heterooligomeric protein complex required for mvb sorting. Developmental Cell 3, 271–282. [PubMed: 12194857]

Buysse D, Pfitzner A-K, West M, Roux A and Odorizzi G (2020). The ubiquitin hydrolase Doa4 directly binds Snf7 to inhibit recruitment of ESCRT-III remodeling factors in S. cerevisiae. J Cell Sci 133,.

Che S, El-Hodiri HM, Wu C-F, Nelman-Gonzalez M, Weil MM, Etkin LD, Clark RB and Kuang J (1999). Identification and Cloning of Xp95, a Putative Signal Transduction Protein in Xenopus Oocytes*. Journal of Biological Chemistry 274, 5522–5531.

Dupré S and Haguenauer-Tsapis R (2001). Deubiquitination step in the endocytic pathway of yeast plasma membrane proteins: crucial role of Doa4p ubiquitin isopeptidase. Mol Cell Biol 21, 4482–4494. [PubMed: 11416128]

Giddings TH (2003). Freeze-substitution protocols for improved visualization of membranes in high-pressure frozen samples. Journal of Microscopy 212, 53–61. [PubMed: 14516362]

Hanson PI, Roth R, Lin Y and Heuser JE (2008). Plasma membrane deformation by circular arrays of ESCRT-III protein filaments. Journal of Cell Biology 180, 389–402.

Ho B, Baryshnikova A and Brown GW (2018). Unification of Protein Abundance Datasets Yields a Quantitative Saccharomyces cerevisiae Proteome. Cell Systems 6, 192–205.e3. [PubMed: 29361465]

Johnson N, West M and Odorizzi G (2017). Regulation of yeast ESCRT-III membrane scission activity by the Doa4 ubiquitin hydrolase. MBoC 28, 661–672. [PubMed: 28057764]

Katzmann DJ, Babst M and Emr SD (2001). Ubiquitin-Dependent Sorting into the Multivesicular Body Pathway Requires the Function of a Conserved Endosomal Protein Sorting Complex, ESCRT-I. Cell 106, 145–155. [PubMed: 11511343]

Kerppola TK (2006). Design and implementation of bimolecular fluorescence complementation (BiFC) assays for the visualization of protein interactions in living cells. Nat Protoc 1, 1278–1286. [PubMed: 17406412]

Kieffer C, Skalicky JJ, Morita E, De Domenico I, Ward DM, Kaplan J and Sundquist WI (2008). Two Distinct Modes of ESCRT-III Recognition Are Required for VPS4 Functions in Lysosomal Protein Targeting and HIV-1 Budding. Developmental Cell 15, 62–73. [PubMed: 18606141]

Kim J, Sitaraman S, Hierro A, Beach BM, Odorizzi G and Hurley JH (2005). Structural Basis for Endosomal Targeting by the Bro1 Domain. Developmental Cell 8, 937–947. [PubMed: 15935782]

Longtine MS, M. A Iii, Demarini DJ, Shah NG, Wach A, Brachat A, Philippsen P and Pringle JR (1998). Additional modules for versatile and economical PCR-based gene deletion and modification in Saccharomyces cerevisiae. Yeast 14, 953–961. [PubMed: 9717241]

Losko S, Kopp F, Kranz A and Kölling R (2001). Uptake of the ATP-Binding Cassette (ABC) Transporter Ste6 into the Yeast Vacuole Is Blocked in the doa4 Mutant. MBoC 12, 1047–1059. [PubMed: 11294906]

Luhtala N and Odorizzi G (2004). Bro1 coordinates deubiquitination in the multivesicular body pathway by recruiting Doa4 to endosomes. Journal of Cell Biology 166, 717–729.

MacDonald C, Buchkovich NJ, Stringer DK, Emr SD and Piper RC (2012). Cargo ubiquitination is essential for multivesicular body intralumenal vesicle formation. EMBO reports 13, 331–338. [PubMed: 22370727]

McCullough J, Fisher RD, Whitby FG, Sundquist WI and Hill CP (2008). ALIX-CHMP4 interactions in the human ESCRT pathway. Proceedings of the National Academy of Sciences 105, 7687–7691.

Mierzwa BE, Chiaruttini N, Redondo-Morata L, Moser von Filseck J, König J, Larios J, Poser I, Müller-Reichert T, Scheuring S, Roux A, et al. (2017). Dynamic subunit turnover in ESCRT-III assemblies is regulated by Vps4 to mediate membrane remodelling during cytokinesis. Nat Cell Biol 19, 787–798. [PubMed: 28604678]

Nickerson DP, West M and Odorizzi G (2006). Did2 coordinates Vps4-mediated dissociation of ESCRT-III from endosomes. Journal of Cell Biology 175, 715–720.

Nickerson DP, West M, Henry R and Odorizzi G (2010). Regulators of Vps4 ATPase Activity at Endosomes Differentially Influence the Size and Rate of Formation of Intralumenal Vesicles. MBoC 21, 1023–1032. [PubMed: 20089837]

Odorizzi G, Babst M and Emr SD (1998). Fab1p PtdIns(3)P 5-Kinase Function Essential for Protein Sorting in the Multivesicular Body. Cell 95, 847–858. [PubMed: 9865702]

Odorizzi G, Katzmann DJ, Babst M, Audhya A and Emr SD (2003). Bro1 is an endosome-associated protein that functions in the MVB pathway in Saccharomyces cerevisiae. Journal of Cell Science 116, 1893–1903. [PubMed: 12668726]

Pashkova N, Gakhar L, Winistorfer SC, Sunshine AB, Rich M, Dunham MJ, Yu L and Piper RC (2013). The Yeast Alix Homolog Bro1 Functions as a Ubiquitin Receptor for Protein Sorting into Multivesicular Endosomes. Developmental Cell 25, 520–533. [PubMed: 23726974]

Richter C, West M and Odorizzi G (2007). Dual mechanisms specify Doa4-mediated deubiquitination at multivesicular bodies. The EMBO Journal 26, 2454–2464. [PubMed: 17446860]

Richter CM, West M and Odorizzi G (2013). Doa4 function in ILV budding is restricted through its interaction with the Vps20 subunit of ESCRT-III. Journal of Cell Science 126, 1881–1890. [PubMed: 23444383]

Row PE, Liu H, Hayes S, Welchman R, Charalabous P, Hofmann K, Clague MJ, Sanderson CM and Urbé S (2007). The MIT Domain of UBPY Constitutes a CHMP Binding and Endosomal Localization Signal Required for Efficient Epidermal Growth Factor Receptor Degradation *. Journal of Biological Chemistry 282, 30929–30937.

Saksena S, Wahlman J, Teis D, Johnson AE and Emr SD (2009). Functional Reconstitution of ESCRT-III Assembly and Disassembly. Cell 136, 97–109. [PubMed: 19135892]

Schmidt MHH, Dikic I and Bögler O (2005). Src Phosphorylation of Alix/AIP1 Modulates Its Interaction with Binding Partners and Antagonizes Its Activities*,. Journal of Biological Chemistry 280, 3414–3425.

Schöneberg J, Lee I-H, Iwasa JH and Hurley JH (2017). Reverse-topology membrane scission by the ESCRT proteins. Nat Rev Mol Cell Biol 18, 5–17. [PubMed: 27703243]

Swaminathan S, Amerik AY and Hochstrasser M (1999). The Doa4 Deubiquitinating Enzyme Is Required for Ubiquitin Homeostasis in Yeast. MBoC 10, 2583–2594. [PubMed: 10436014]

Teis D, Saksena S and Emr SD (2008). Ordered Assembly of the ESCRT-III Complex on Endosomes Is Required to Sequester Cargo during MVB Formation. Developmental Cell 15, 578–589. [PubMed: 18854142]

Teis D, Saksena S, Judson BL and Emr SD (2010). ESCRT-II coordinates the assembly of ESCRT-III filaments for cargo sorting and multivesicular body vesicle formation. The EMBO Journal 29, 871–883. [PubMed: 20134403]

Vida TA and Emr SD (1995). A new vital stain for visualizing vacuolar membrane dynamics and endocytosis in yeast. Journal of Cell Biology 128, 779–792.

Webster BM, Colombi P, Jäger J and Lusk CP (2014). Surveillance of Nuclear Pore Complex Assembly by ESCRT-III/Vps4. Cell 159, 388–401. [PubMed: 25303532]

Wemmer M, Azmi I, West M, Davies B, Katzmann D and Odorizzi G (2011). Bro1 binding to Snf7 regulates ESCRT-III membrane scission activity in yeast. Journal of Cell Biology 192, 295–306.

Wollert T, Wunder C, Lippincott-Schwartz J and Hurley JH (2009). Membrane scission by the ESCRT-III complex. Nature 458, 172–177. [PubMed: 19234443]

Yang B, Stjepanovic G, Shen Q, Martin A and Hurley JH (2015). Vps4 disassembles an ESCRT-III filament by global unfolding and processive translocation. Nat Struct Mol Biol 22, 492–498. [PubMed: 25938660]

Synopsis

At yeast endosomes, membrane scission by the ESCRT-III complex is regulated through binding of the Snf7 subunit to Doa4, a ubiquitin hydrolase. Another ESCRT-III subunit, Vps20, also binds Doa4. This study shows that Vps20 inhibits Doa4 interaction with Snf7 and that inhibitory binding of Vps20 to Doa4 is relieved by Bro1, a cofactor that regulates Doa4 function.

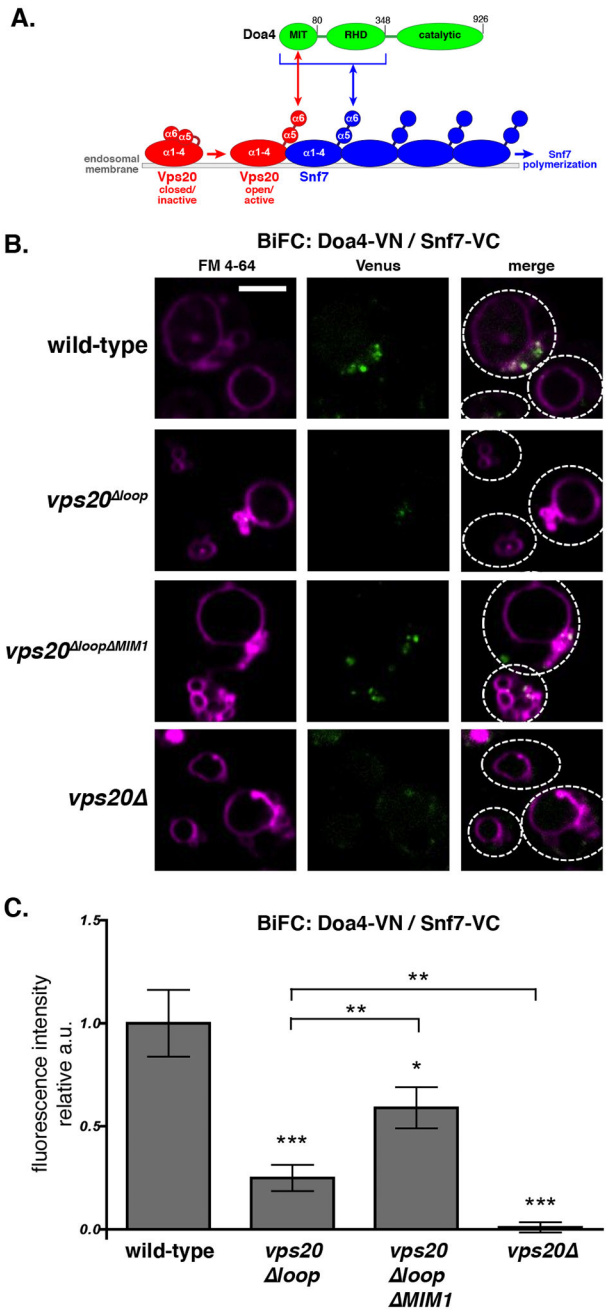

Figure 1. Vps20 antagonizes Doa4 interaction with Snf7 at yeast endosomes

(A) Schematic diagram of Doa4, with its domain structure and corresponding amino acid positions indicated. Doa4 domain interactions with the Vps20 and Snf7 subunits of ESCRT-III are depicted. Also shown is Vps20 transition from its closed/inactive conformation to its open/active state that nucleates Snf7 polymerization. MIT, Microtubule Interacting and Trafficking domain; RHD, Rhodanese Homology Domain; catalytic, ubiquitin hydrolase domain. (B) Live-cell BiFC fluorescence microscopy images showing the interaction of Doa4-VN and Snf7-VC in the indicated yeast strains. Vacuole membranes are stained with FM 4–64. Dashed lines indicate cell outlines. Scale bar, 4 μm. (C) Quantification of the

mean BiFC fluorescence per cell based on ≥3 independent experiments with the cells shown in (B). Error bars represent the standard error of the mean (SEM); *$P \leq 0.05$, **$P \leq 0.01$, *$P \leq 0.001$.

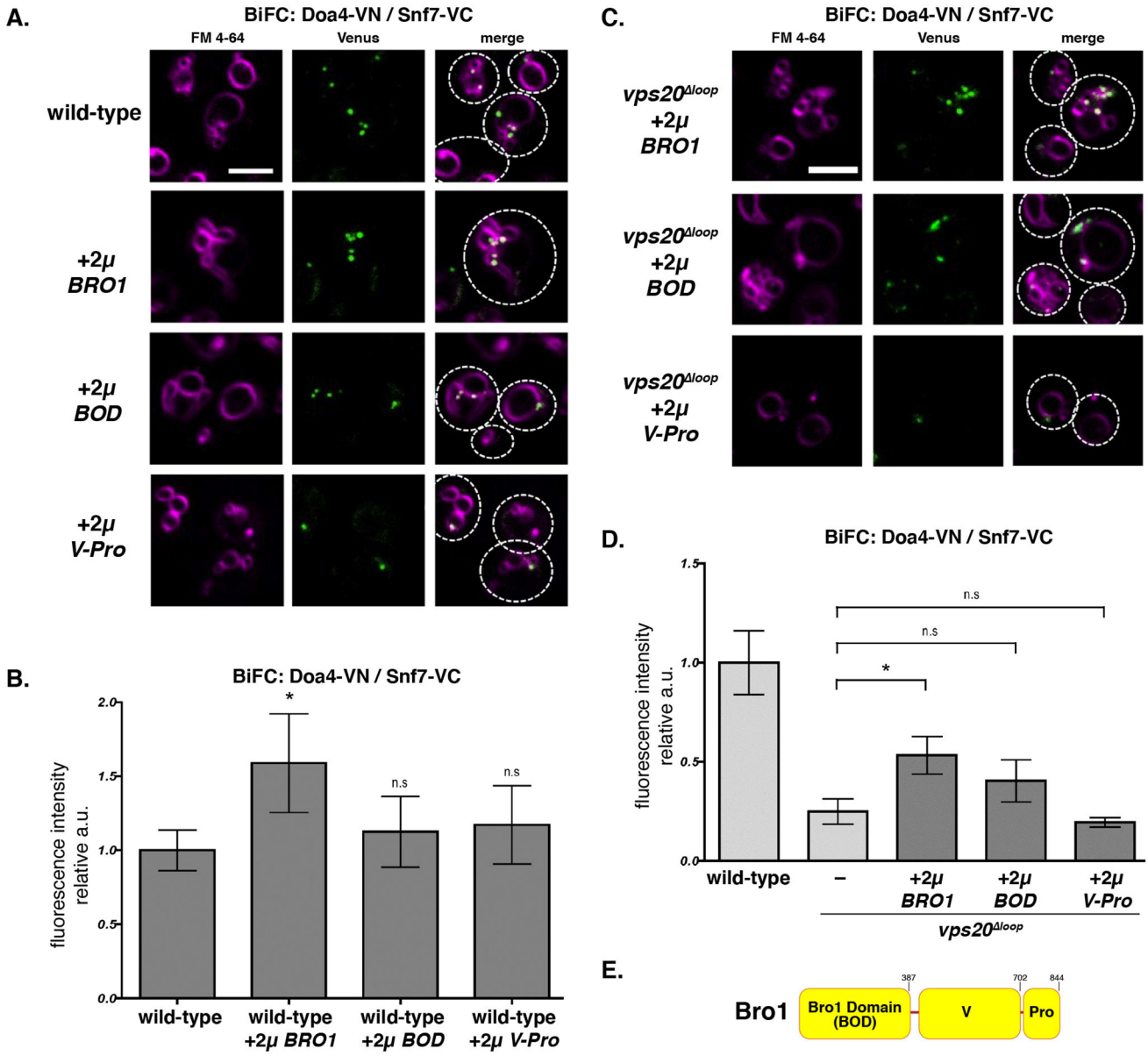

Figure 2. Doa4 interaction with Snf7 in vivo is promoted by Bro1

(A, C) Live-cell BiFC fluorescence microscopy images showing the interaction of Doa4-VN and Snf7-VC in the indicated yeast strains without or with overexpression of wild-type *BRO1* or mutant *bro1* alleles using a high-copy-number (2μ) plasmid. BOD, Bro1 Domain; V-Pro, Bro1 V Domain and proline-rich region. Vacuole membranes are stained with FM 4–64. Dashed lines indicate cell outlines. Scale bar, 4 μm. (B, D) Quantification of the mean fluorescence per cell based on ≥3 independent experiments with the cells shown in (A) and (C), respectively. Error bars represent the SEM; *$P \leq 0.05$, n.s., not significant. (E) Schematic diagram of Bro1, with its domain structure and corresponding amino acid positions indicated.

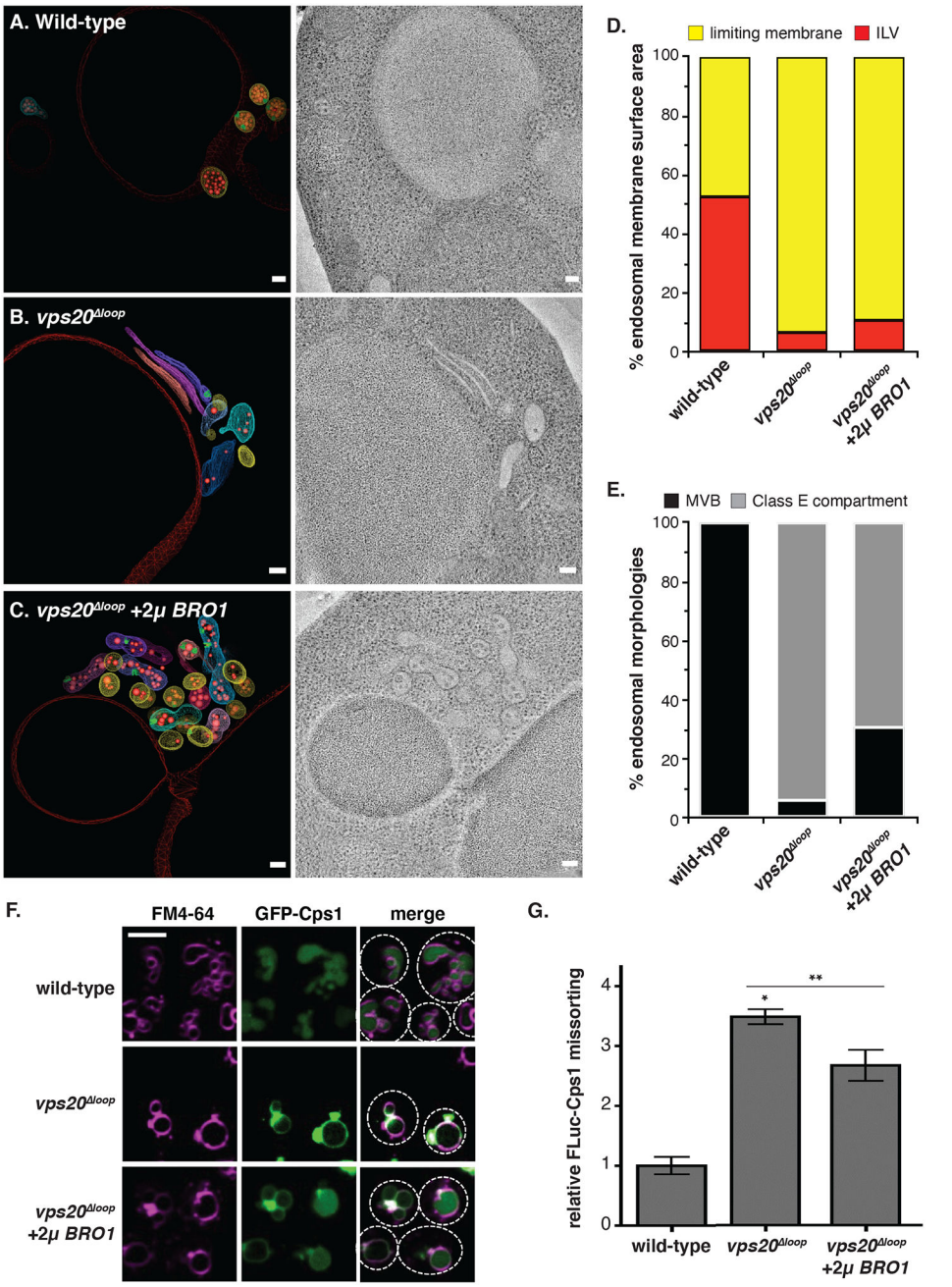

Figure 3. *BRO1* overexpression rescues ILV budding and cargo sorting in *vps20*$^{\Delta loop}$ cells

(A-C) Cross-sectional tomographic slices and 3D models obtained using electron tomography of 250-nm thick sections of the indicated yeast strains. In each model, detached ILVs are traced in red and limiting endosomal membranes are traced in different colors. Scale bars, 100 nm. (D) Quantification of the surface areas of ILVs versus limiting membranes in endosomes modeled by tomography. (E) Quantification of the number of MVBs versus class E compartments observed by thin-section EM. (F) GFP-Cps1 localization in the indicated strains stained with FM 4–64. Dashed lines indicate cell outlines. Scale bar, 4 μm. (G) Quantification of the missorting of FLuc-Cps1 using the

LUCID assay. A higher FLuc-Cps1 / RLuc ratio indicates an increase in defective ILV cargo sorting. Error bars represent the SEM (*$P \leq 0.01$) from 3 independent experiments with 3 technical replicates in each experiment.

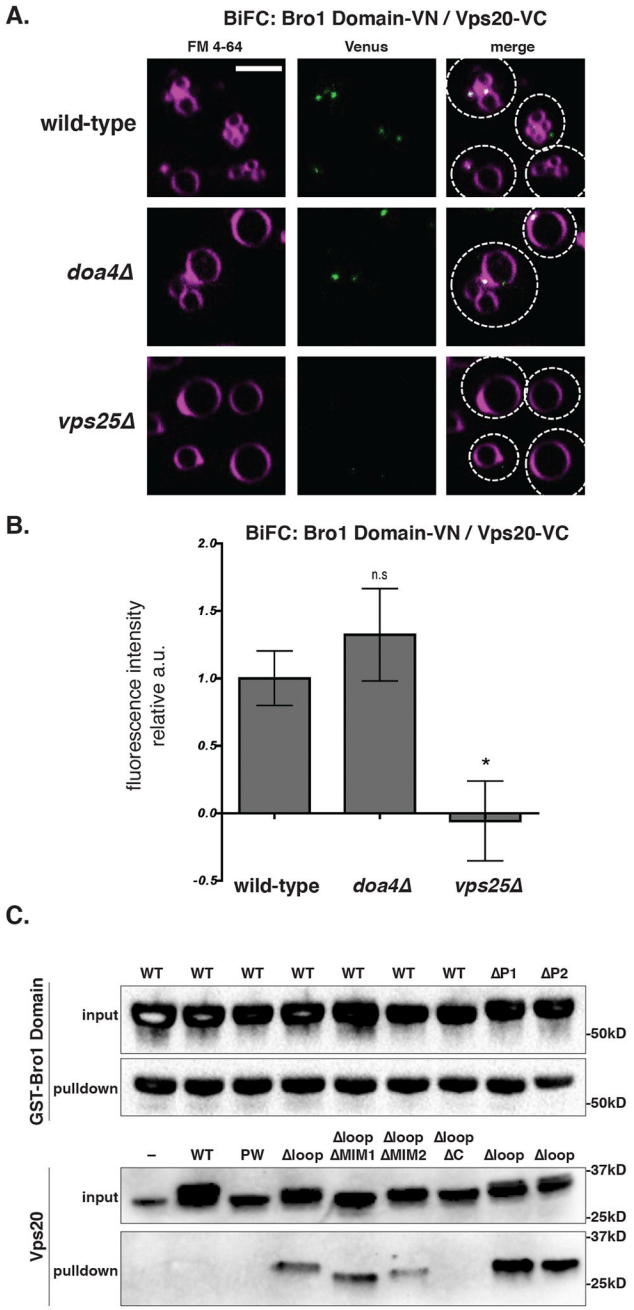

Figure 4. Bro1 directly binds Vps20

(A) Live-cell BiFC fluorescence microscopy images showing the interaction of Bro1 Domain-VN and Vps20-VC in the indicated yeast strains. Vacuole membranes are stained with FM 4–64. Dashed lines indicate cell outlines. Scale bar, 4 μm. (B) Quantification of the mean fluorescence per cell based on ≥3 independent experiments with the cells shown in (A). Error bars represent the SEM; *$P \leq 0.05$, n.s., not significant. (C) Western blotting after affinity isolation of GST-Bro1 Domain incubated with lysates of bacteria expressing wild-type or mutant Vps20 proteins. Input and affinity isolated proteins were blotted with anti-GST or anti-Vps20 antiserum. Molecular weights are indicated at the right.

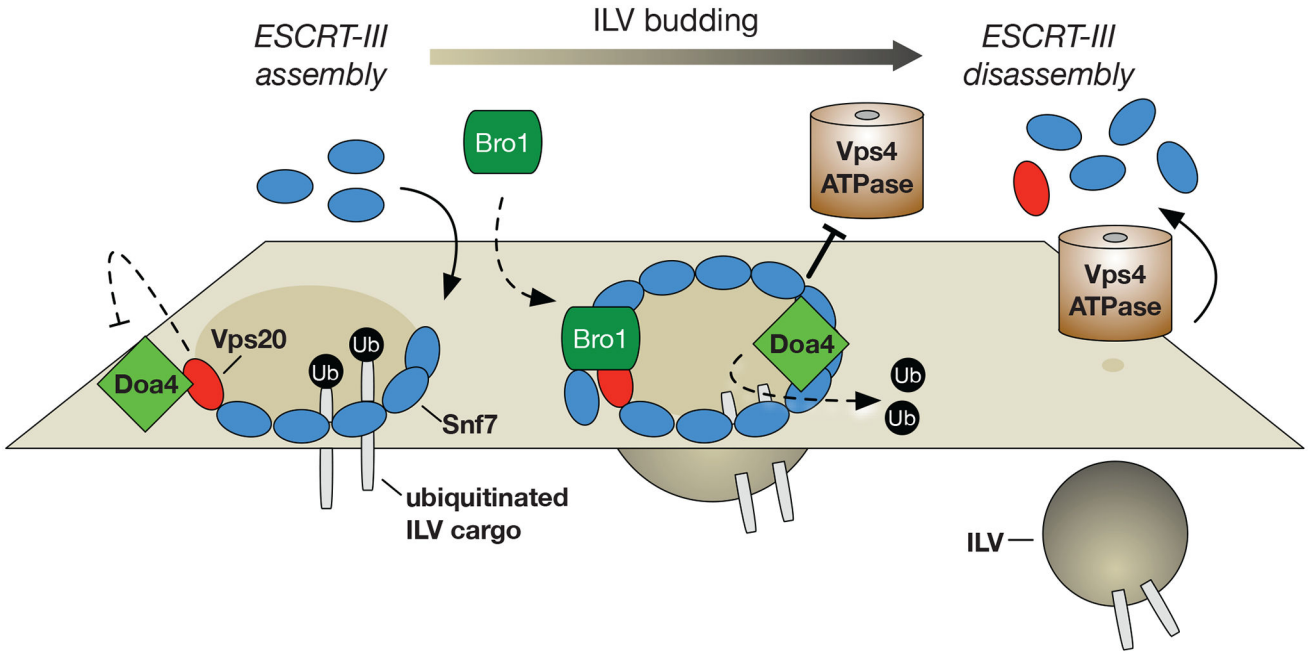

Figure 5. Working hypothesis of Bro1 relieving Doa4 from inhibition by Vps20

Doa4 is the ubiquitin hydrolase that deubiquitinates ILV cargoes. Doa4 also binds directly to Snf7, which inhibits membrane scission by ESCRT-III. Both of these functions of Doa4 are inhibited through its interaction with the Vps20 subunit of ESCRT-III, the latter of which initiates ESCRT-III assembly by nucleating Snf7 polymerization. Our study shows that Bro1, like Doa4, directly binds Vps20 and that Bro1 overexpression in vivo both inhibits Doa4 interaction with Vps20 and promotes Doa4 interaction with Snf7. These observations suggest a working hypothesis in which Bro1 binding to Vps20 relieves Doa4 from Vps20-mediated inhibition, thereby facilitating Doa4 function in the deubiquitination of ILV cargoes and the regulation of ESCRT-III membrane scission activity.

Table 1.

Yeast strains used in this study

Strain	Genotype	Reference
SEY6210	*MATα leu2–3,112 ura3–52 his3Δ200 trp1-Δ901 lys2-Δ801 suc2-Δ9*	Robinson et al., 1988
DBY9	SEY6210; *bro1Δ::TRP1*	This study
GOY461	SEY6210; *snf7-VC::KANMX6 doa4-VN::HIS3*	Buysse et al., 2020
GOY581	SEY6210; *vps20-VC::KANMX6; bro1$^{1–387}$-VN::HIS3*	This study
MRY30	SEY6210; *vps20Δ::HIS3*	Russell et al., 2012
MWY25	SEY6210; *snf7$^{L231A;L234A}$::KANMX6*	Wemmer et al., 2011
DCBY83	SEY6210;*vps20-VC::KANMX6;bro1$^{1–387}$-VN::HIS3; snf7Δ::LEU2*	This study
DCBY86	SEY6210; *vps20-VC::KANMX6; bro1$^{1–387}$-VN::HIS3; vps25Δ::LEU2*	This study
DCBY87	SEY6210; *vps20-VC::KANMX6; bro1$^{1–387}$-VN::HIS3; doa4Δ::LEU2*	This study
DCBY93	SEY6210; *vps20-VN::HIS3; doa4-VC::KANMX6; vps4Δ::TRP1*	This study
DCBY107	SEY6210; *snf7-VC::KANMX6 doa4-VN::HIS3; vps20Δ::LEU2*	This study
DCBY171	SEY6210; *snf7$^{L231A;L234A}$::KANMX6; bro1Δ::TRP1*	This study
DCBY173	SEY6210; *snf7$^{L231A;L234A}$::KANMX6 vps20Δ::HIS3*	This study

Table 2.

Plasmids used in this study

Plasmid	Genotype	Reference
pRS202	*URA3 Ap* ^{R}	Christianson et al., 1992
pRS426	*URA3* Ap^{R} *2μ*	Christianson et al., 1992
pRS413	*HIS3 Ap*^{R} *CEN*	Christianson et al., 1992
pRS414	*TRP1 Ap*^{R} *CEN*	Christianson et al., 1992
pRS415	*LEU2 Ap*^{R} *CEN*	Christianson et al., 1992
pRS416	*URA3 Ap*^{R} *CEN*	Christianson et al., 1992
pST39	*Ap* ^{R}	Tan, 2001
pCR180	*LEU2 ApR CEN* (*pRS415) SNA3-GFP*	Wemmer et al., 2011
pDCB17	*LEU2 Ap*^{R} *CEN (pRS415) GFP-CPS1*	Buysse et al., 2020
pDCB21	*Ap*^{R} *(pST39) Vps20*$^{\Delta 48–59; P216D; L217D}$*; GST-BRO1*$^{1–387}$	This study
pDCB35	*Ap*^{R} *(pST39) Vps20*$^{\Delta 48–59; L188D}$ *; GST-BRO1*$^{1–387}$	This study
pDCB45	*Ap*^{R} *(pST39) Vps20*$^{\Delta 48–59}$ *; GST-BRO1*$^{1–387; I144D; L336D}$	This study
pDCB47	*Ap*^{R} *(pST39) Vps20*$^{\Delta 48–59}$ *; GST-BRO1*$^{1–387; F318D; I319D; Y320D}$	This study
pDCB51	*Ap*^{R} *(pST39) Vps20*$^{1–170;\Delta 48–59}$ *; GST-BRO1*$^{1–387}$	This study
pDCB61	*TRP1 Ap*^{R} *CEN (pRS414) VPS20*$^{\Delta 48–59}$	This study
pDCB63	*TRP1 Ap*^{R} *CEN (pRS414) VPS20*$^{\Delta 48–59; P216D; L217D}$	This study
pDCB101	*HIS3 Ap*^{R} *CEN (pRS413) BRO1*$^{I144D; L336D}$	This study
pDCB102	*HIS3 Ap*^{R} *CEN (pRS413) BRO1*$^{PSVF-AAAA}$	This study
pDCB103	*URA3* Ap^{R} *2μ (pRS202) DOA4*	This study
pDCB104	*URA3* Ap^{R} *2μ (pRS202) DOA4*$^{YPFL-AAFA}$	This study
pEE2	*TRP1 Ap*^{R} *CEN (pRS414) VPS20*	Babst et al., 2002
pGO216	*URA3* Ap^{R} *2μ (pRS426) BRO1*	Wemmer et al., 2011
pGO263	*HIS3* Ap^{R} *CEN (pRS413) BRO1*	Luhtala & Odorizzi, 2004
pGO642	*URA3* Ap^{R} *2μ (pRS426) BRO1*$^{388–844}$	Johnson et al., 2017
pGO735	LEU2 Ap^{R} (pDN615) *PGK1*$_{pr}$*::RLuc CPS1*$_{pr}$*::FLuc-SNA3*	This study
pGO817	*Ap*^{R} *(pST39) Vps20*$^{\Delta 48–59}$	Johnson et al., 2017
pGO818	*Ap*^{R} *(pST39) GST-Doa4*$^{2–80}$	Johnson et al., 2017
pGO826	*Ap*^{R} *(pST39) Vps20*$^{\Delta 48–59}$*; GST-Doa4*$^{2–80}$	Johnson et al., 2017
pGO840	*Ap*^{R} *(pST39) Vps20; GST-BRO1*$^{1–387}$	This study
pGO843	*Ap*^{R} *(pST39) Vps20*$^{P183W; P189W; P192W}$ *; GST-BRO1*$^{1–387}$	This study
pGO844	*Ap*^{R} *(pST39) Vps20*$^{\Delta 48–59}$*; GST-BRO1*$^{1–387}$	This study
pGO896	*Ap*^{R} *(pST39) Vps20*$^{\Delta 48–59; L188D}$ *; HA-BRO1*$^{1–387}$	This study
pGO897	*Ap*^{R} *(pST39) Vps20*$^{\Delta 48–59; L188D}$ *; GST-Doa4*$^{2–80}$*; HA-BRO1*$^{1–387}$	This study
pMWM3	*URA3* Ap^{R} *2μ (pRS426) BRO1*$^{1–387}$	Wemmer et al., 2011
pMW32	*URA3 Ap*^{R} *CEN (pRS416) SNF7*$^{L231A; L233A}$	Wemmer et al., 2011